Article:
Kwokal, A, Čavužić, D and Roberts, KJ (2013) Surface adsorbed templates for directing the crystal growth of entacapone as monitored using process analytical techniques. Crystal Growth and Design, 13 (12). 5324 - 5334. ISSN 1528-7483

https://doi.org/10.1021/cg401188c

Surface adsorbed templates for directing the crystal growth of Entacapone as monitored by ATR-UVvis spectroscopy and FBRM†

Ana Kwokal[1], Dražen Čavužić[1] and Kevin J. Roberts[2]*

[1]Pliva Croatia Ltd., Teva Pharmaceuticals, Research and Development, Prilaz baruna Filipovića 29, Zagreb, Croatia.

[2]Institute of Particle Science and Engineering and Institute of Process Research and Development, School of Process, Environmental and Materials Engineering, University of Leeds, LS2 9JT, Leeds, UK.

**communicating author*

† Paper first presented at the 10th International Workshop of the Crystal Growth of Organic Materials (CGOM10), University of Limerick, Ireland 11-14 June 2012.

Key words: crystallisation kinetics, surface template, Entacapone, FBRM, ATR-UVvis, spectroscopy, seeding

Abstract

Crystallisation of Entacapone (E-2-cyano-N,N-diethyl-3-(3,4-dihydroxy-5-nitrophenyl) propenamide) in acetone solution at 500 mL scale using a self-assembled layer of the host material on Au(111) as a seeding template was studied and monitored using ATR-UVvis spectroscopy and FBRM. The data reveal that the template promotes crystal growth at lower supersaturations and at an increased rate when compared to experiments carried out without the template. The resulting crystals prepared are also found to have superior properties with respect of those produced without the template, notably having a much narrower crystal size distribution, a greatly superior perfection and a more equant crystal morphology. These observations are rationalised by the template providing a sympathetic surface for the promotion of crystallisation in an analogous mechanism to that associated with conventional seeding, but with the added advantage of conferring a well-ordered, easily reproducible and more robust process.

Introduction

It is well understood that nucleation is an initial and crucial step for the crystal growth process, and one that, in principal, is governed by the presence of active surface sites.[1,2] It has also been revealed that the presence of structurally-ordered templates during crystallisation can direct the nucleation process through enabling specific interactions between the active sites and crystallising material at the interface[1-5] as well as within the bulk solution resulting in the formation of materials with improved solid-state properties[6]. Several types of interfacial templates have been demonstrated in this respect, notably single crystal surfaces[1,7], self-assembled layers[3,4,8] and Langmuir-Blodgett films[9], all generally considered to be ordered molecular surface systems.

The pre-requisite properties needed for an effective surface template to be able to induce nucleation is for the templating surface to enable the specific adsorption of the molecules to be crystallised onto the template. These could be either the same molecules as those to be crystallised or to contain functional groups which mimic those of the crystallising species. In this respect, the use of surface templates is, in principle, analogous to the use of crystalline seeds to promote the nucleation and growth of a targeted solid form. The use of such templates to provide an alternative seeding approach is the one adopted in this study. In this work, template surfaces having the same molecules as those required to be crystallised have been immobilised on to a substrate surface to provide a seeding environment to direct crystallisation.

Any metallic or a dielectric surface can, in principle, exhibit an electrical potential difference with respect to the bulk solution and thus, in doing so, can attract molecules such as solute, solvent or impurities to adsorb, either as a monomolecular self-assembled layer or

as 2D or 3D ad-layer. It is also well-known that many organic molecules can strongly adsorb on metal surfaces such as gold, platinum or even at stainless steel. In the latter case such materials are commonly used in the construction of industrial crystallising reactors and/or their internals such as baffles, impellers or process probes. Previous studies have shown that crystallisation behavior can be strongly influenced by the material used in construction of crystallisation vessel and their scale size[10,11]. Indeed, it is a common and anecdotal observation in industrial crystallization practice that the first crystallisation in a freshly cleaned reactor can be quite different in nature with respect to subsequent crystallisations (see e.g. reference[6]). This is often related to surface effects, e.g. by the formation of an ad-layer of adsorbed molecules which impacts on the crystallisation process through promoting heteronucleation at the ad-layer surface. It is also well-known that such adsorbed molecules can sometimes persist in being bound to surfaces even after their rinsing by solvent and/or heating the solution above its solubility limit. In industrial practice this is manifested in the challenges associated with the validation of cleaning between successive batch processes. Such effects, which have not as yet attracted significant academic study, perhaps reflects the strong interfacial bonding between the functional groups typical found in organic molecule such as –SH[4,12],-CN[6], -NH_3[13] or -SCN[14] to the surface. However, such effects and their impact on a heteronucleation can be difficult to characterize, reproducibly control and scale-up. As a result the practical exploitation of such interfacial processes can be problematic in terms of their utility for crystallisation optimization and control.

Seeding has long been used to control heteronucleation and direct the crystallisation processes[15]. However, this approach provides significnt challenge in terms of effecting a reproducible process as significant variations in seed quality are possible depending on the methods used for seed production.[16] A number of steps can be used for the preparation of

seed materials including milling, blending, grinding, sieving, and washing[16], and all of these have the potential to suffer from problems associated with the materials irreproducibility. Reflecting this perspective, the use of well-ordered surface templates offers an alternative and potentially improved way of delivering the benefits attracted by the seeding process, and in doing so offers the potential benefit in providing a much more reproducible seeding surface, thus facilitating a much more controlled crystallisation process.

In-situ process analytical techniques (PAT) can be used to characterize, monitor and control crystallisation process (e.g. [17,18,19]) and in particular case presented here have been applied to assess the performance of template in mediating the crystallisation process. In particular, PAT is useful to define how these templates influence the crystallisation process kinetics as well as the concomitant impact on the physical and chemical properties of the resulting crystals. For this purpose, ATR-UVvis spectroscopy coupled with Focused Beam Reflectance Measurement (FBRM) provides an ideal combination. The advantages of the former for the measurement of solution concentration lies in its fibre optic based technology which enables an easy connection of the in-process probe to the spectrometer. UVvis spectroscopy is also an ideal analytical technique for the measurement of strongly absorbing solutions, where e.g. standard transmission probes cannot be used.[20,21] Similarly, FBRM provides an effective technique for the assessment of the crystallisation process, particularly the *in-situ* characterization of the crystal size and growth rate.

In previous work[6], it has been demonstrated that the pharmaceutical compound Entacapone spontaneously adsorbes on a single crystal surface of gold from the solution phase and forms an orderly arrangement. Moreover, these ordered ad-layers have been shown to make a significant impact on the crystallisation process through inducing nucleation at significantly lower supersaturations and directing the solid-state properties of the resulting

crystals resulting in the formation of the stable polymorphic form which is crystallised with a much narrower crystal size distribution and superior crystal perfection and morphology. In this study[6] the metastable zone width and nucleation kinetics were characterized with and without the presence of a nucleation (seeding) template. In this paper the work is extended using an ATR-UVvis spectroscopy and FBRM, to access the templates influence of crystal growth kinetics.

2. MATERIALS AND METHODOLOGY

2.1 Materials

Entacapone, (E)-2-cyano-N,N-diethyl-3-(3,4-dihydroxy-5- nitrophenyl) propenamide, was provided by courtesy of PLIVA Croatia, with about 99.9% purity. The crystallisation solvent was acetone which was obtained from Kemika. Single crystals of polymorphic form A were prepared by evaporative crystallisation from a 30 mg/mL acetone solution.

The template for the crystallisation studies was an Au(111) thin film sputtered on to a Gold Arrandee^{TM} borosilicate glass. (The borosilicate glass had a thickness of 0.7 +/- 0.1 mm and was prepared with a chromium buffer layer of 2.5 +/- 1.5 nm thick followed by a final gold layer of 250 +/- 50 nm thick with the sizes of 11x11 +/- 0.2 mm). The samples were flame annealed to achieve Au(111) terraces.

2.2 Experimental set-up

Batch-cooling crystallisation experiments in acetone solvent were carried out using jacketed 150 mL and 500 mL reaction vessels agitated by a magnetic stirrer and a Teflon-coated retreat curved impeller operated at 180 rpm, respectively. The reactors were equipped with a temperature probe, and an ATR-UVvis probe for monitoring the solute concentration. A

Lasentec® D600L FBRM probe (Mettler) was used for monitoring the crystal size for the 500 mL reactor system. A thermostatically-controlled bath (Julabo F32) was used for the cooling/heating control of the reactors. Temperature data logging was facilitated through the use of Easy Temp software[22]. The ATR-UVvis spectroscopy system consisted of the immersion ATR probe fitted with an optic cable (Hellma GmbH) integrated with a Varian Carry 50 spectrophotometer equipped with the Carry WinUV data acquisition software.

2.3 Preparation of surface template

The procedure for the preparation of the self-assembled layer template of Entacapone onto the gold substrate was carried out by immersing the Au thin film on glass into an under-saturated solution (30 mg/mL) of Entacapone in acetone for about 12 hours, after which it was immediately rigorously rinsed with acetone to remove any non-adsorbed material.

2.4 Crystallisation procedures

Both polythermal and isothermal methods were used to characterise the crystallisation behaviour of Entacapone.

The polythermal crystallisation experiments were carried out using the 150 mL reactor using heating/cooling cycles, at different linear cooling rates (typically 0.25°, 0.5°, and 1°C/min) and concentrations (60, 70, 80 and 90 mg/mL). From this the metastable zone widths (MSZW) were determined.

The isothermal crystallisation experiments, with and without the template, were carried out using the 500 mL reactor and at a solution concentration of 70 mg/mL. The solution cooling rate to the set temperature was 1°C/min, this reflecting the cooling capacity of the cooling thermostatic bath. The solution was cooled down from 50°C, at which, all the solute was

dissolved, to the desired crystallisation temperatures of 15℃, 7℃ or 5℃. Spontaneous crystallisation was detected using FBRM whilst the solution concentration was measured using ATR-UVvis spectroscopy. The isothermal temperature ranges were set within the metastable zone determined from the polythermal measurements.

The isothermal crystallisation experiments using the template were carried out using this same procedure with the template introduced into the crystallising solution at 50 ^{o}C and held vertically above the impeller prior to cooling.

The reactors for both polythermal and isothermal experiments were rigorously cleaned between each run, including all internal surfaces, by wiping with a cloth and by ultrasound cleaning.

2.5 Process analytical experiments

ATR-UVvis measurements were performed by dipping the ATR-UVvis probe into the reactor vessel. For the best performance, the ATR probe was located in the high turbulence zone, above the impeller. Due to a very small penetration depth of the light beam, the probe used for the measurements was cleaned to avoid contamination. In order to achieve a better and more reproducible performance, the probe was always positioned in the same position which was ensured by the position of the sample ports located in the cover of the reactor. The spectral range of the UV measurements, were between 220 nm and 500 nm and an acquisition time of 60 s per scan was used. Measurement of the blank (pure solvent), as well as the “zero correction” (correction for the instrument noise), were regularly carried out.

For calibration purposes, the concentrations of five different solutions were prepared (40; 50; 60; 70 and 80 mg/mL) by weighing the appropriate amounts of Entacapone, dissolving in acetone at an appropriate temperature and cooling down to 30℃. The measurements were

performed as quickly as possible to avoid any undesired crystallisation reflecting the fact that level of concentration and temperature solution was supersaturated. For the temperature calibration, the solutions (60, 70, 80 and 90 mg/mL) were measured over the temperature range of 50℃ – 15℃. A simple in house computer pr ogram written in MatLab was developed for calibration purposes.

X-ray power diffraction measurements were carried out using a Philips X'Pert diffractometer with zero background holders, CuKα source (λ = 1.54 Å), continuous scanning at 0.04 ^{o}/s, a 2θ scan range from 0-40°, step size 0.017° and counti ng time 1.7 min/step.

Single crystals of Entacapone were morphologically indexed at room temperature (297 K), using an Oxford Diffraction Xcalibur diffractometer with CuKα radiation (λ = 1.54 Å). The diffraction data were collected with a Sapphire CCD detector, over a range from 2θ = 3.4–61.4°. An omega-scan data were collected using Crys AlisPro, (Oxford Diffraction Ltd.), Version 1.171.32.18, (CrysAlis171.NET)[23] and SHELXS97[24] was used for data analysis. Entacapone Form A crystallises in a triclinic system crystal (Cambridge Crystallography Data Centre, reference code OFAZUQ).

Focus beam reflectance measurements were simultaneously recorded together with the ATR-UVvis data. There was no visible attachment of crystals to the probes during the crystallisation process. The only disturbance during the measurement of the signal sometimes arose from the presence of the air bubbles in the solution, but this was only in the temperature range from about 50℃ to 25℃. Special care was taken when cleaning the probe. For every new measurement the tip of the probe, as well as the surrounding metallic surfaces, was thoroughly cleaned by rinsing several times with acetone and wiping the surface with a tissue and a water/acetone mixture. More than a 200 chord lengths were simultaneously measured to produce the chord length distribution. Whilst the measured

chord length distribution is related to the particle size, this correlation is not straightforward due to the fact that the FBRM measures the chord length for all part of the crystal, e.g. corners and edges as well as that relate to the centroid of the sample, i.e. these measurements takes no account of the shape of the crystals. Nonetheless, the technique does provide a useful and effective indication of the on-set of the crystallisation process as well as providing the broad features associated with the development and growth of the resultant crystal formed.

2.6 Solubility

ATR-UVvis spectroscopy was used for solubility determination since the technique enabled the measurement of solute concentration *in-situ*, in the presence of solid particles, without the need for filtration. Direct measurement of solvent concentration in slurry was utilised and found to be beneficial both from an accuracy and practical point of view. Slurries of Entacapone were stirred at temperatures (25, 30, 35, 40 and 45 ^{o}C), each for about 24 hours, and UVvis spectra were taken at the end of mixing period. The absorbance at UVvis peak maxima were used to calculate the solution concentrations, i.e. solubility, according to the calibration model (equation 3).

2.7 Crystal growth rate determination

Crystal growth rates from isothermal crystallisation experiments with and without the presence of the template were determined from the chord length measurements using two different methodologies: initial rate and discretisation. For the initial rate approach the derivative of the chord length over time was calculated over the linear part of median chord length curve, as shown schematically in Figure 1. Based on this, the growth rates were

calculated for the three different supersaturations (σ) associated with isothermal temperatures of 15 ^{o}C, 7 ^{o}C and 5 ^{o}C. In this supersaturation was defined as:

$$\sigma = c / c^* - 1 \qquad (1)$$

An empirical rate equation as expressed through the inter-relationship between the growth rate (G) and supersaturation (σ) was used to assess the mechanistic aspect of the growth:

$$G = k_G \times (z-\sigma)^b \qquad (2)$$

where k_G (μm/min) is the rate constant, b (dimensionless) is the order and z is a correction factor used for discretisation method.

For the discretisation approach both the supersaturation and chord length curves were decomposed into temporal segments from which the mean values were assessed and the continuous relationship between growth rate and supersaturation, throughout the batch process, established.

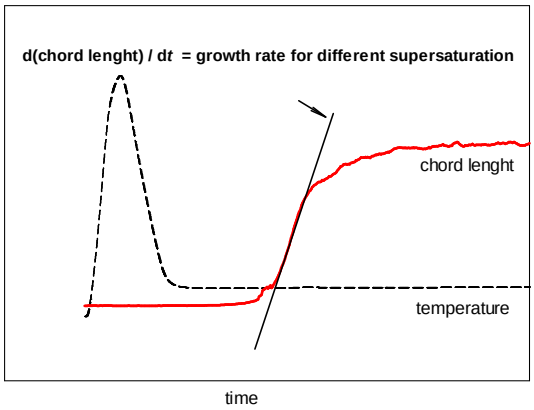

Figure 1. *Schematic diagram highlighting the isothermal data acquisition strategy with temperature (dashed line) and chord length profile (solid red line) taken during a heating-cooling crystallisation showing the part of the FBRM curves used for derivation (slope) determination (solid black line).*

3. RESULTS and DISCUSSION

3.1. ATR UVvis method development

Entacapone/acetone solutions revealed a strong absorbance maxima in UV region at about 310 nm (Figure 2(a)). The baseline of the spectra was not found to shift significantly even in the presence of insoluble particles during the crystallisation process or even for different temperatures.

The ATR-UVvis spectroscopy calibration (Figure 2(b)) shows the correlation between UVvis absorbance intensity and the solute concentration for different concentrations of Entacapone in acetone at 30℃ revealing linear correlation. However, for constant solution concentration, the absorbance was found to increase as a function of temperature decrease, as shown in Figure 2(c). This effect is well known for the ATR and is connected to the change of refractive index[21] due to changes in the path length of the UVvis signal as it passes through the ATR sapphire prism and solution. It was also found that the absorbance as a function of temperature gradient ($\Delta A/\Delta T$) varied with concentration Figure 2(b). However, the dependence of concentration vs. absorbance, absorbance vs. temperature and $\Delta A/\Delta T$ vs. concentration (c) was found to be linearly correlated enabling a multilinear approach to be adopted for calibration model development. This method involved calculating the parameters for A, absorbance, and T, temperature as denoted in calibration model:

$$c = a_1 \times A + a_2 \times T + a_3 \qquad (3)$$

Using this relationship, a multilinear regression analysis yielded the following parameters from the experimental data: $a_1 = 326.69$; $a_2 = 0.323$; $a_3 = -18.05$

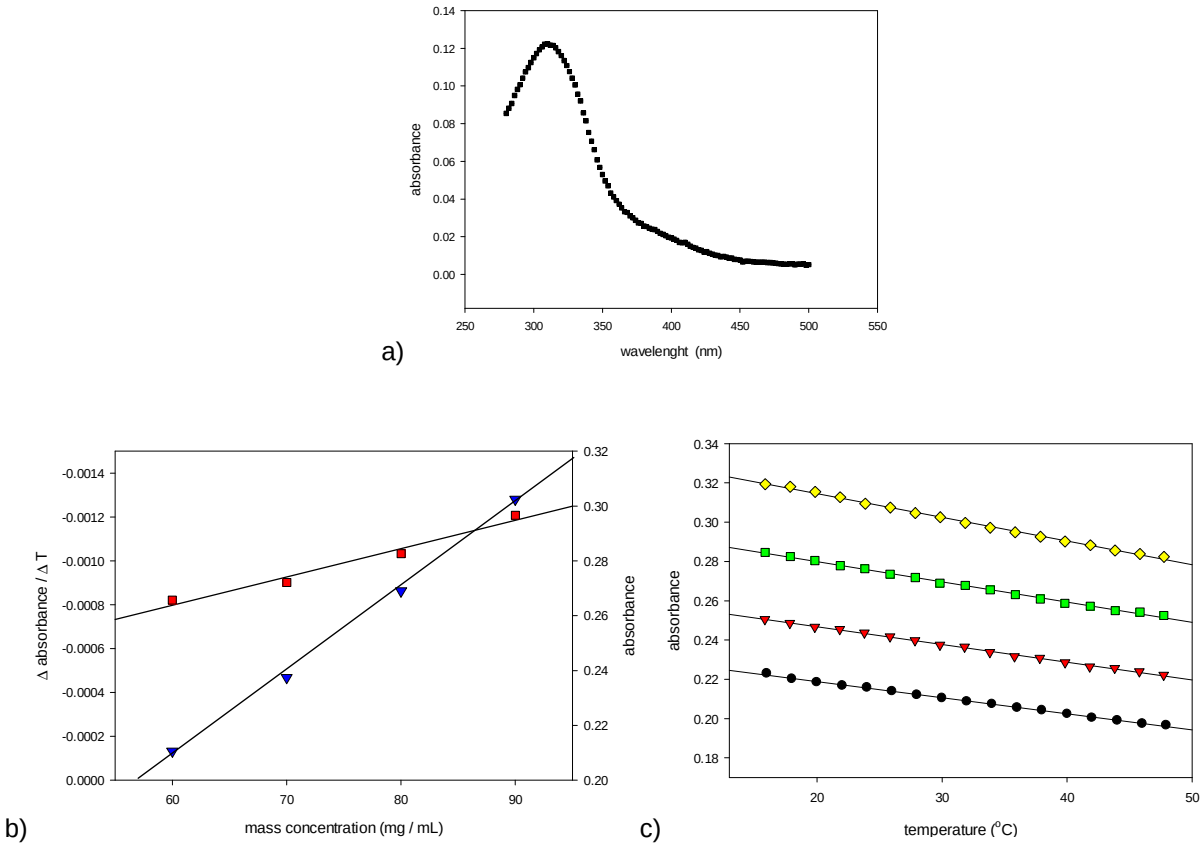

Figure 2. *ATR-UVvis spectra (a) and calibration: b) absorbance at peak maxima vs. mass concentration at 30℃ (triangles) and variation of ∆absorbance/∆T with the concentration (squares); c) absorbance at peak maxima vs. temperature for the 60, 70, 80 and 90 mg/mL (bottom to top)*

3.2 Solubility

The solubility was assessed using polythermal method with data being presented in Figure 3 in comparison to the ideal solubility behaviour given by:

$$\ln x = \frac{\Delta_f H}{R}\left(\frac{1}{T_m} - \frac{1}{T}\right) \qquad (4)$$

where x is molar concentration; R is gas constant, ΔH_f (enthalpy of fusion) = 201.5 J/g and T_m (melting temperature) = 166.5 ^oC[6]. The solubility of Entacapone in acetone solution was found to be several orders of magnitude higher than for the mixed aqueous/acetone solution studied previously[6] and close to the ideal predicted (Figure 3), revealing that solute/solute

interactions are preferred for both solvents but that solute/solvent interactions in acetone is perhaps a bit stronger in the absence of water.

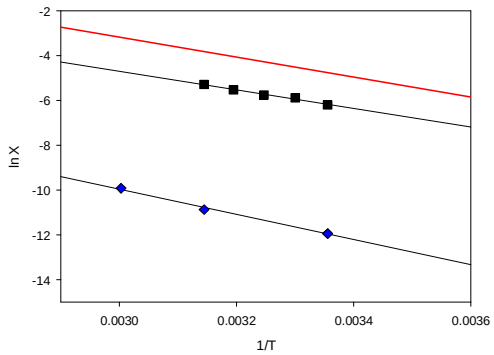

***Figure 3**. Solubility of Entacapone in acetone (black squares) and water with 12 % acetone (blue squares) as measured in-situ using ATR-UVVIS presented as van't Hoff plot showing its relationship with ideal solubility behaviour (red line).*

3.3 Polythermal crystallisation at 150mL scale

Figure 4(a) shows a 3D plot of the ATR-UVvis spectra measured as a function of temperature recorded during cooling crystallisation. The UVvis absorbance peak maxima as a function of temperature is given in Figure 4(b), together with its solution concentration as calculated according to equation (3). The data reveals that the UVvis absorbance maxima increases slightly with temperature decrease, but starts to rapidly decrease following crystallisation with the inflection point indicating the onset of crystallisation (Figure 5(a)). The crystallisation onset can be best observed as a peak in the plot of supersaturation versus temperature, as shown in Figure 5(b). The metastable zone widths (MSZW) were measured at various cooling rates and solute concentrations with representative examples being shown in Figure 6. The MSZW was found to vary significantly with concentration cooling rate. Typical MSZW for concentration of 90 mg/mL was about 30 ^{o}C, while for lower concentration rise up to 45 ^{o}C and 51 ^{o}C for 0.5 ^{o}C/min and 1 ^{o}C/min cooling rate respectively.

Such wide MSZWs are not that uncommon for organic systems[25,26]. Presumably at the lower solute concentrations the propensity for solute-solute interactions in the solution decreases, hence lowering the probability of crystallisation. Similarly, the increase in MSZW with increasing cooling rate is typical of the behaviour of materials which do not spontaneously nucleate easily[27,28]. In such cases, the rate of production of available solute from the decrease in solubility due to temperature lowering is not matched by the nucleation rate resulting in a lowering of the crystallisation on-set.

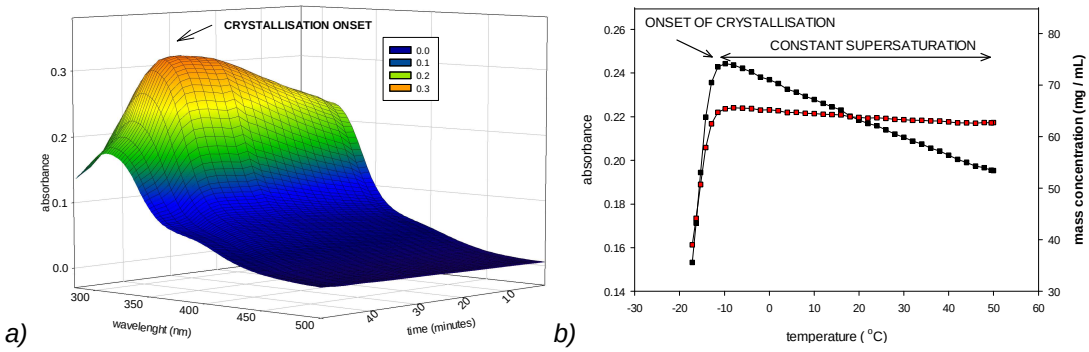

***Figure 4**. ATR-UVvis spectral data and its analysis: (a) 3D plot showing the in-process absorbance vs. wavelength vs. temperature ATR-UVVIS spectra as recorded during the cooling crystallisation of Entacapone in acetone solution. (b) Plot of the ATR-UVVIS peak maxima as a function of temperature as measured (black) and re-calculated (red) taking into account the temperature effect to the concentration according to equation (3).*

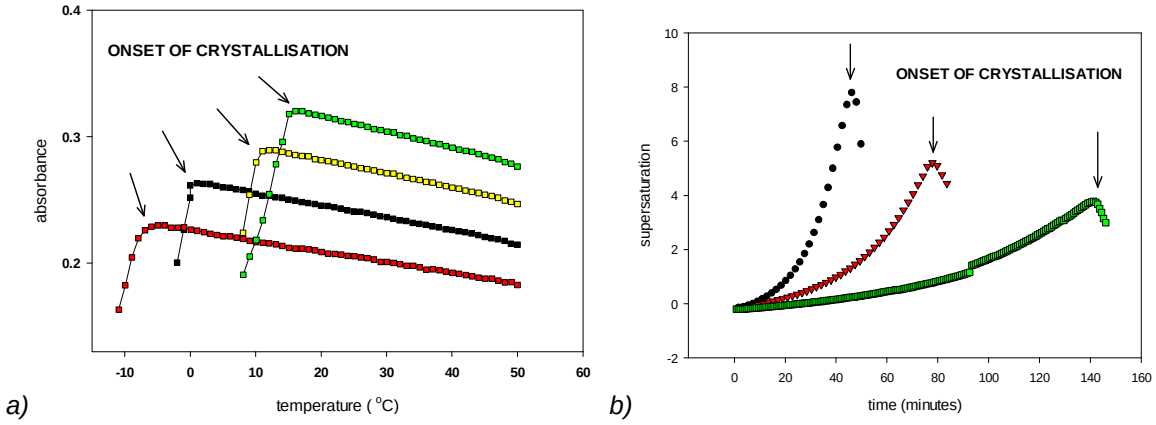

***Figure 5**. Polythermal cooling crystallisation runs presented as plots of (a) absorbance at peak maxima of UVvis spectra vs. temperature for 0.5℃/min cooling rate and the mass concentration of 60; 70; 80; 90 mg/mL (bottom to top) and as b) solutions supersaturation vs. time as a function of cooling rate; 1 °C/min; 0.5 °C/min; 0.25 °C/min (from left to the right).*

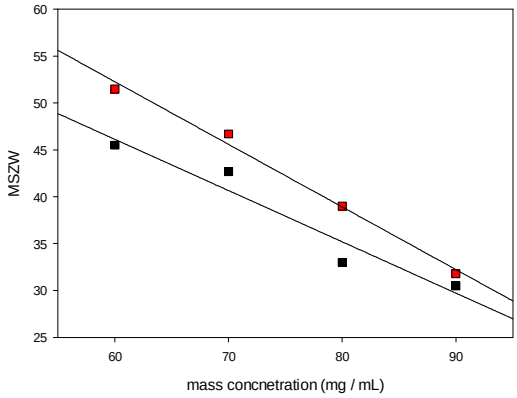

***Figure 6**. Plot of metastable zone width as a function of concentration and cooling rate; 0.5 ^{o}C/min (red) and 1 ^{o}C/min (black).*

3.4 Isothermal crystallisation without template

The MSZW obtained at 150 mL together with the associated determination of the solubility data enabled a range of isothermal crystallisation runs to be carried out at 15℃, 7℃ and 5℃. The data, presented in Figure 7, shows an over lay of the median chord length from the FBRM measurements together with the UVvis absorbance spectra both measured as function of time during three successive heating and cooling cycles. The inflection points for the respective absorbance and FBRM curves at about 200, 700 and 1100 minutes indicate the onset of crystallisation for each crystallisation run. Comparison between onset detection by the UVvis and FBRM, shown in Figure 8, reveals FBRM to be slightly more sensitive with regard to the detection of the onset of crystallisation when compared to the UVvis measurements. The UVvis and FBRM data were analysed to estimate crystal growth rate (*G*). The inter- relationship between mean chord length change and supersaturation revealing that the best fit to the equation (2) gives a value of k_G of 0.96 μm/min and *b* of 1.28, consistent with a linear (diffusion controlled) crystal growth[29].

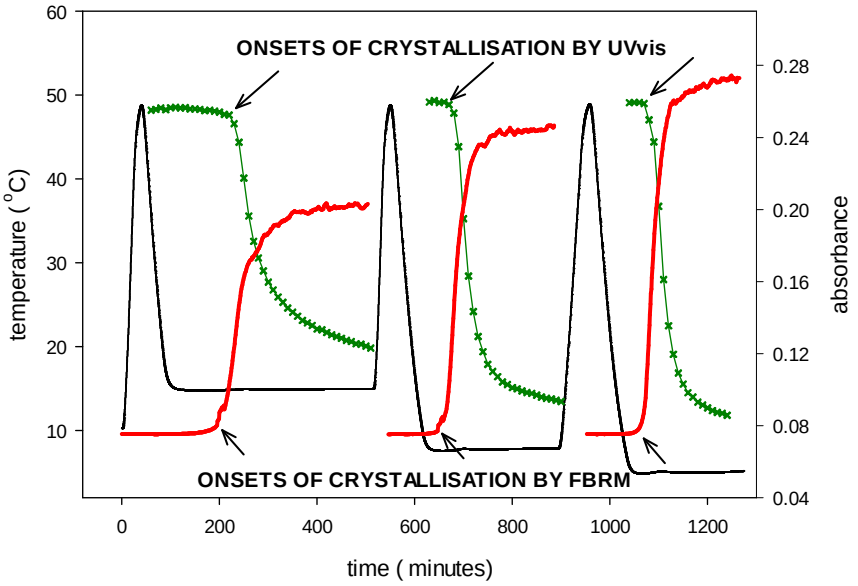

***Figure 7**. FBRM median chord length (red), UV/VIS absorbance (green) and temperature (black) data for a 70 mg/mL Entacapone/acetone solution associated with crystallisation during three consecutive crystallisation cycles.*

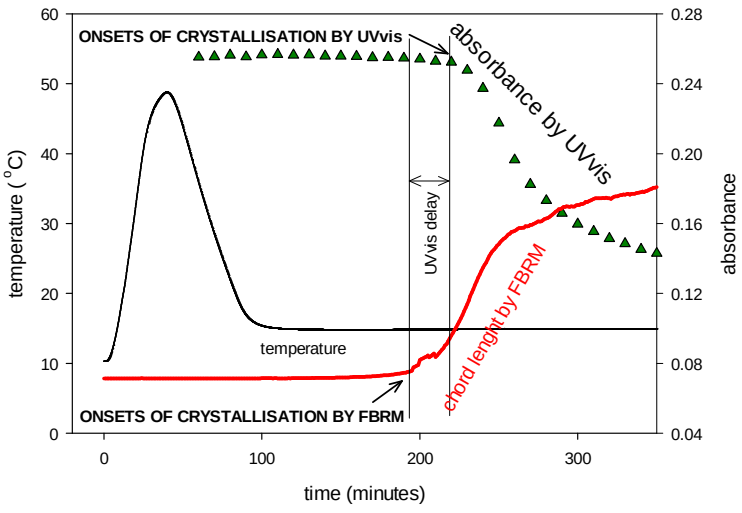

***Figure 8**. Zoomed area from **Figure** 7 where the correlation, in terms of crystallisation onset, between FBRM and UV/VIS data clearly reveals the sensitivity of the FBRM approach.*

Caution though is needed in terms of over interpreting these results mindful of the fact that the supersaturation decreases during the growth period and thus this kinetic assessment may only being indicative rather than be too quantitative. In addition, the chord length measurements are only loosely correlated to the actual crystal size and the growth mechanism is also likely to be highly face (hkl) specific and that these factors can be expected to have an effect. Nonetheless, this work demonstrates the added value gained through use of a combination of process analytical techniques, in particular when highlighting their utility in probing the influence of processing conditions on the product quality.

3.5 Isothermal crystallisation with template

Figure 9 shows ATR-UVvis and FBRM data measured during isothermal crystallisation in the presence of the template which is overlaid with the data obtained from crystallisation without template. Examination of the broad feature of supersaturation versus time curve (Figure 9(a)) demonstrates that the onset of crystallisation without template begins at about 50 minutes for crystallisation temperature of 8℃, after exhibitin g fast decrease in supersaturation during the cooling period and supersaturation plateau later on. The chord length versus time curve was found to be in rough coincidence in their respective onset points of crystallisation with supersaturation and increase relatively slowly within the first 130 minutes of crystallisation and later progress rather fast until reaching the constant value.

However, in the presence of the template the crystallisation process was found to be initiated significantly earlier (at about 40 minutes). Examination of the chord length measurements reveals the growth process to proceed faster and reaching a constant value within 150 minutes when chord length starts to retard. Overall, the kinetics of the crystal growth process was found to differ significantly between these two experiments with the reduction in the

crystallisation onsets points and increased growth velocities confirming the ability of the template to induce nucleation at a lower supersaturation and to subsequently promote growth. Examination of the initial stages of growth close to its onset (b) shows the process in more detail which characterises the template effect as one which enhances the growth rate, enabling a shorter induction time and a faster de-supersaturation rate in comparison to the absence of the template.

Figure 10 shows the experimental rate data presented in a more mechanistic form, i.e. in terms of growth rate versus supersaturation. The former is the derivative with respect to time of the mean chord length. The latter involves a temporal discretisation of the de-supersaturation curve enabling the kinetics to be assessed over the whole crystallisation process. This is in contrast to the initial rate approach adopted earlier (section 3.4), e.g. in the analysis presented in Figure 10(b) (data presented as green triangles). This analysis (Figure 10(a)) highlights the easier nucleation and subsequent higher growth rates that result from the presence of the template. In contrast, in the absence of the template the crystallisation process appears to be inhibited for a time which would be consistent with the presence of some kind of a dead zone after which both the growth rate and duration is seen to rapidly increase. Towards the end of the batch runs the growth rate both with and without template were found to fall away (fall off zone), this reflecting the depletion of the solution supersaturation. An examination of the reaction rates is given in Figure 10(b) and Table 1. In this, the supersaturation is normalised to zero in order for an effective comparison of the two methodologies. The data seems to indicate that the growth rate without the template is slightly higher than with the template with both values appearing to be lower than those calculated for the initial rate approach. This is consistent with the assumption that crystals prepared on the template once being faceted, proceed to grow with similar fashion to the

case of crystallisation without the template but differ significantly in their early stages of growth. In this respect, it is worth noting that in a continuous crystallisation process perhaps encompassing supersaturation control[18,19], the growth rate could be sustained for longer period to produce materials over a much wider range of supersaturations and crystal sizes.

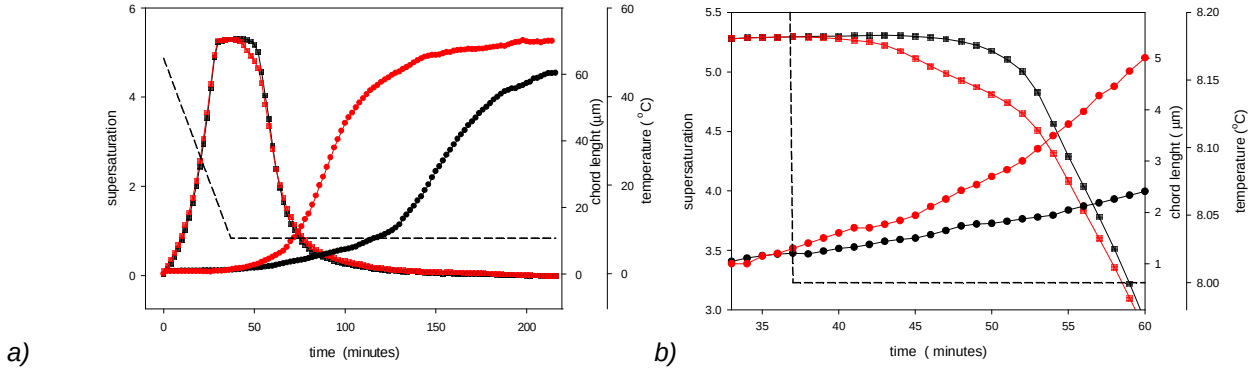

***Figure 9**. In-process data with and without template: (a) UVvis absorbance (squares), chord length (circles), and temperature (dashed line) profile for 70 mg/mL cooling crystallisation in the 500 mL reactor in the absence (black) and presence (red) of the template. (b) enlarged area highlighting the early stage of crystallisation.*

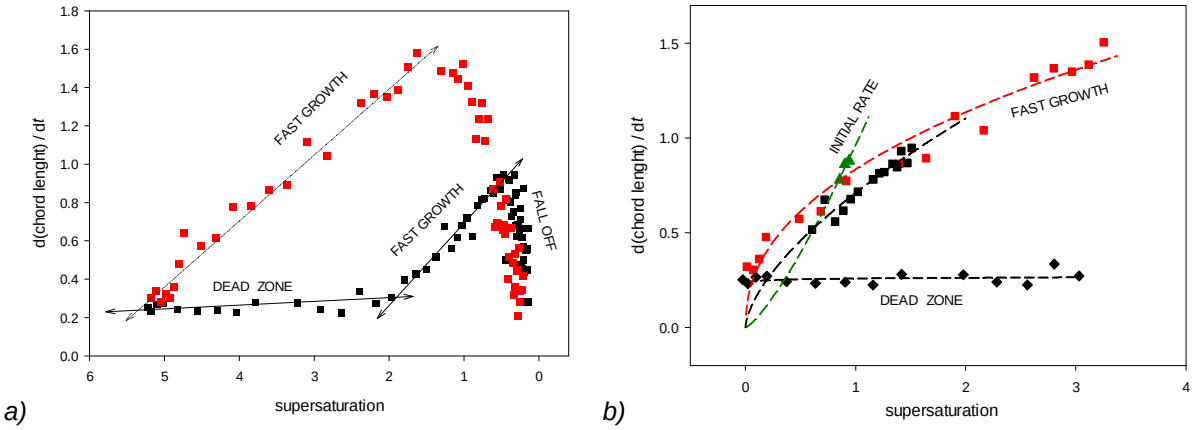

***Figure 10** Mechanistic rate data: (a) Plot of the change in mean chord length as a function of supersaturation for a 70 mg/mL concentration of Entacapone in acetone solution in the absence (black) and presence of the template (red). (b) Enlargements of growth rate with template (red squares) and without template (black squares) normalised to zero supersaturation; together with plot of growth rate (green triangles) for data taken from consecutive crystallisation runs without template, by initial growth rate together with data fitted (dashed line) according to equation (2).*

Table 1. *Kinetic parameters derived from the growth rate vs. supersaturation measurements.*

	Without template		*With template*	
	k_b / μm min^{-1}	*b*	k_b / μm min^{-1}	*b*
Initial rate	0.96	1.28	*NA*	
Discretisation (dead zone)	0.26	0.02	*NA*	
Discretisation (fast growth)	0.71	0.63	0.83	0.44

3.6 Characterisation of the Entacapone crystals obtained with and without template

Figure 11 show micrographs taken of the crystals harvested from the crystallisation experiments which have carried out with and without presence of the template. The crystals obtained in the presence of the template were found to have a narrower size distribution and to be of a much higher crystal quality notably exhibiting a thickened plate-like morphology with a well-defined crystal shape and smooth edges. On the contrary the crystals prepared from crystallisation without the template were found to have a wide size distribution and to be of a much lower crystal quality, e.g. often displaying poorly-defined morphology with often rough edges and broken surfaces. However, the mean crystal size from both experiments was found to be rather similar, with a median diameter of about 400 µm. Figure 12 shows indexation of the crystal habit surfaces as determined from a single crystal grown from acetone by solvent evaporation. This highlights the main crystal planes present in a plate-like crystal morphology which is dominated by the (001) crystal plane together with much smaller (101), (100), (01-1) and (010) faces. Powder XRD (Figure 13) examination of the Entacapone grown with and without the presence of the template both confirmed the crystals to be of form A. Both XRD patterns were found to be very similar albeit with slight differences in peaks intensities, as shown in Figure 13(a). Further analysis of the data showed that peak at 11.9 degrees 2θ to be associated with diffraction from the (100) plane which was not visible in the crystals harvested from the run without template revealing that this plane (100) was not

developed Figure 13(b). However, the same peak was found to be well-pronounced in the diffraction pattern of crystals obtained with the template, implying that Entacapone crystals have developed (100) plane. The (100) plane is positioned at the side of crystal in respect to largest (001) plane and is the plane which best characterised the thickness of the overall crystal. The differences in morphology of crystals are found to be consistent with nucleation being promoted by template which initiates the initial stages of the nucleation process and subsequent growth at a lower supersaturation. Examination of the crystal micrographs reveals that the growth rate of specific faces has been altered, i.e. previously slow growing crystal direction has been developed more at lower supersaturations, consequently changing the overall crystal morphology.

(a) 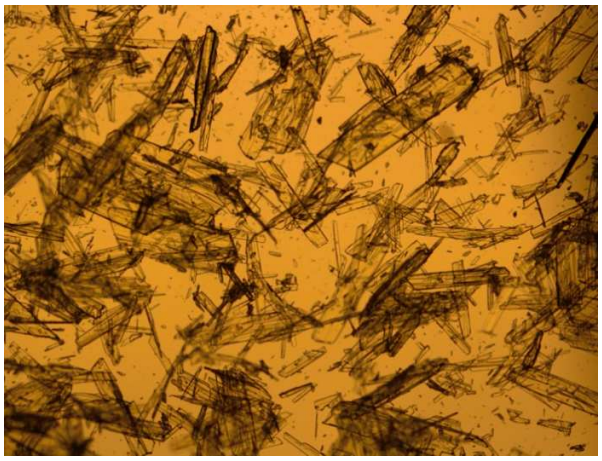 (b) 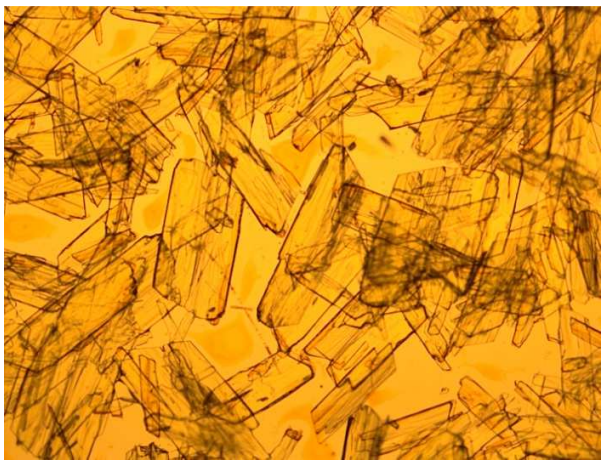

Figure 11. *Photomicrograph of crystal harvested after cooling crystallisation of 70 mg/mL Entacapone / acetone in the first crystallisation run without (a) and with template (b).*

The observation, both this work and previously the published data[6], is that bulk crystallisation in the presence of the template results in a more narrow crystal size distribution than in the absence of the template is highlighted significantly. The reasons for this are not completely clear but perhaps the template provides an alternative interface to pre-orientate and assemble molecules through physical adsorption and hence by this mechanism promotes the

heteronucleation process. Following this, the hydrodynamic conditions presumably then lead to the detachment of these initial crystal/nuclei when they reach a critical size. This, in turn, frees up a site on the template for a subsequent nucleation event and so on. Why nucleation takes place on the template and not through the more typical secondary nucleation mechanisms of contact breeding, attrition etc. is also an open question but perhaps it reflects the high quality of molecular ordering present in the templates surface against the other competing secondary nuclei environments where the structural order might not be so high.

Furthermore, the fact that template surface is being continually refreshed by the crystal detachment process probably effects to maintain a constant source of preferred sites for a subsequent nucleation, growth and detachment cycle. Clearly though, this analysis is speculative and further and more detailed studies are needed to confirm this proposed mechanistic pathway.

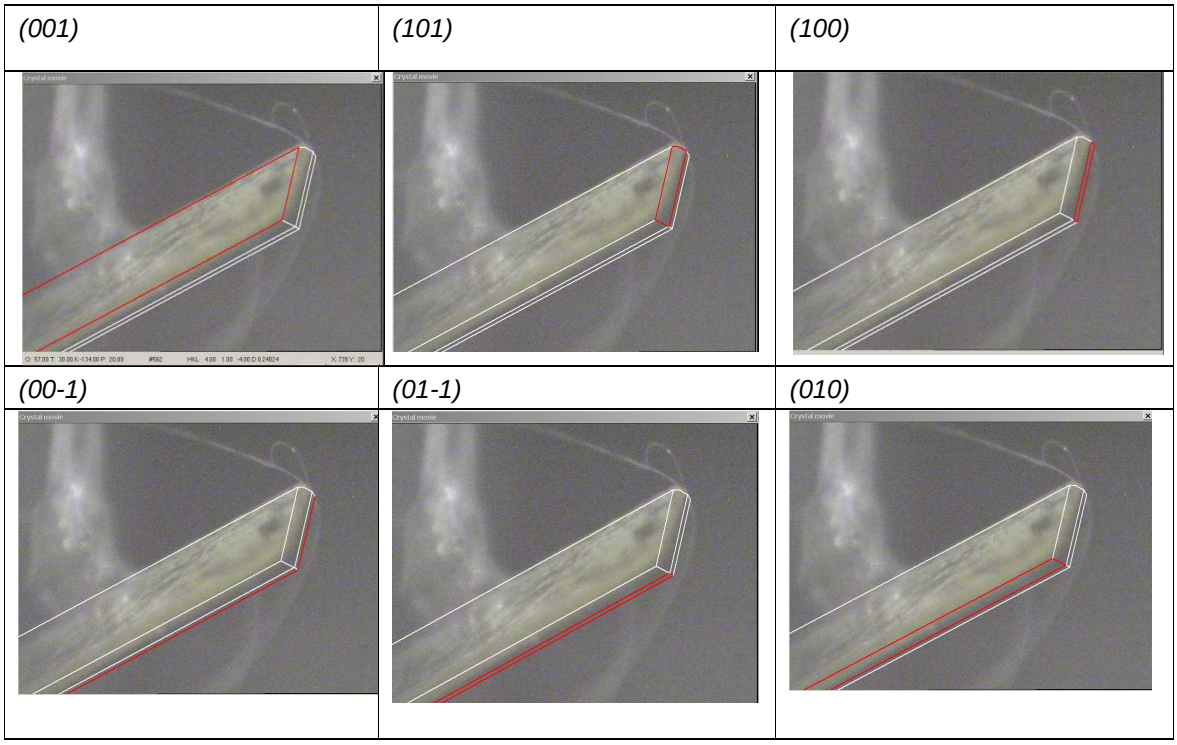

Figure 12. *Single crystal indexed of Entacapone form A; main crystal planes, defined by Miller indexes and outlined red.*

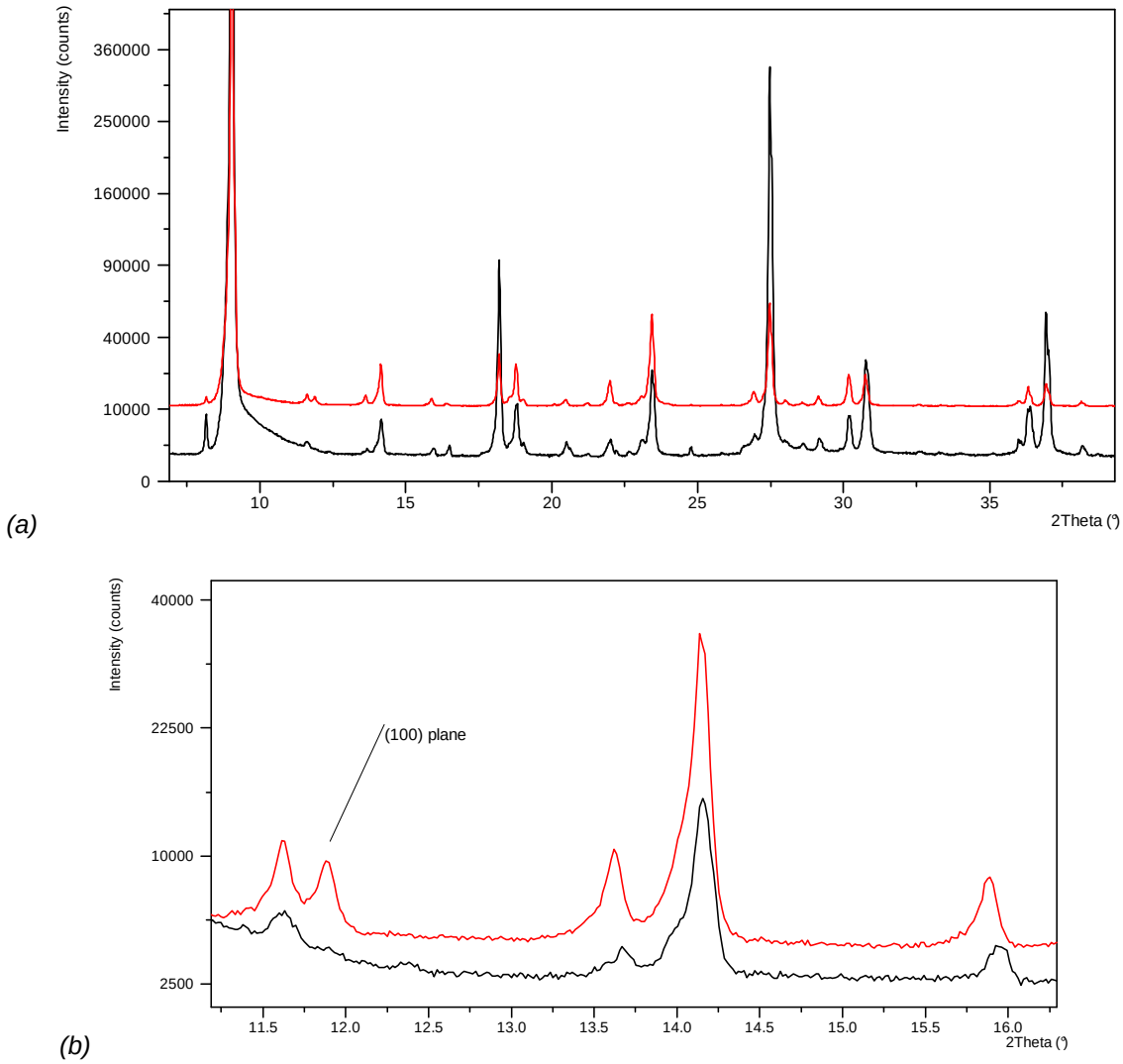

Figure 13. *a) XRDs of Entacapone crystals harvested after cooling crystallisation of 70 mg/mL Entacapone / acetone in the first crystallisation run with template (red, upper) and without template (black, lower) b) Zoomed area.*

4. Conclusion

Crystallisation of Entacapone in acetone solution with and without the use of nucleation seeding template was studied through the application of PAT techniques for crystallisation monitoring.

The surface template, consisting of adsorbed layer of Entacapone on Au(111) single crystal surface was found to serve as an effective nucleation promoter, i.e. as an alternative seeding

material. This kind of seed provides an ordered surface with self-assembled molecules through following order of the adsorbent molecule layer on the Au(111) single crystal surface. A significant influence of the template on the onset of crystallisation, the crystal growth mechanism and the crystal morphology was revealed.

Crystals harvested after crystallisation in the presence of template were found to have a narrow size distribution, to be thicker, to have much smoother crystal edges and a more desired crystal morphology. It was also notable, the narrower crystal size distribution in the presence of seeding template suggested that a predominant for heteronucleation process at the template surface compares to the usual secondary nucleation process.

The study revealed that adsorbed molecules of Entacapone on Au(111) surface provided sympathetic surface for promoting nucleation i.e. nuclei at the surface which are being swept from the surface by hydrodynamic forces making secondary seed and, thus, influencing the crystallisation in the entire bulk solution. The use of such a well-ordered surface template offers alternative and improved way of seeding due to its well defined surface order, its ability to be reproducibly made at nano-scale and its ability to be renewable and stabile above the solubility point.

This research also reveals tailor made template as being a more controlled way of seeding with the possibility of making an impact on crystal morphology by promoting nucleation at lower supersaturation.

Acknowledgment

Ana Kwokal gratefully acknowledges PLIVA Croatia Ltd. for the financial support during the study leave at the University of Leeds. We grateful acknowledge to Dubravka Šišak from ETH, Zurich for the help with the morphological indexation of Entacapone crystal.

Kevin Roberts also gratefully acknowledges the UK's EPSRC for the support of nucleation research at Leeds through funding the Critical Mass Project Molecules, Clusters and Crystals (grant reference EP/I014446/1).

References

(1) Ward, M. D. *Chem. Rev.* **2001**, *101*, 1697-725.

(2) Myerson, A. S.; Lee, A. *Pat. Appl. WO2006/052995*.

(3) Mitchell, C. A.; Yu, L.; Ward, M. D. *J. Am. Chem. Soc.* **2001**, *123*, 10830-10839.

(4) Hiremath, R.; Basile, J. A.; Varney, S. W.; Swift, J. A. *J. Am. Chem. Soc.* **2005**, *127*, 18321-18327.

(5) Weissbuch, I.; Leiserowitz, L.; Lahav, M. *Curr. Opin. Colloid.* **2008**, *3*, 12-22.

(6) Kwokal, A.; Nguyen, T.; Roberts, J. K. *Cryst. Growth Des.* **2009**, *4*, 4324-4334.

(7) Bonafede, S. J.; Ward, M. D. *J. Am. Chem. Soc.* **1995**, *117*, 7853-7861.

(8) Heywood, B. R. *J .Chem. Soc. Farad.Trans.* **1991**, *87*, 735-743.

(9) Landau, E. M.; Levanon, M.; Leiserowitz, L.; Lahav, M.; Sagiv, J. *Nature* **1985**, *318*, 353-356.

(10) Liang K., White G., and Wilkinson D., Ford L.J. and Roberts K.J., Wood, W.M.L. *Cryst. Growth Des.* **2004**, 2, 1039-1044.

(11) Liang K., White G., and Wilkinson D., Ford L.J. and Roberts K.J., Wood, W.M.L. *Ind EngChem Res* **2004**, *43*, 1227-1234.

(12) Kang, J. F.; Zaccaro, J.; Ulman, A.; Myerson, A. S. *Langmuir,* **2000**, *16*, 3791-3796.

(13) Dressler, D. H.; Mastai, Y. *Cryst. Growth Des.* **2007**, 7, 847-850.

(14) Biljan I.; Biljan T. Vancik H. In 10th European Symposium on Organic Reactivity, Rome, Italy, 2005; Rome, Italy, **2005**.

(15) Beckmann W. *Org. Proc. Res. & Dev.* **2000**, 4, 372-383.

(16) Aamir E.; Nagy Z. K.; Rielly C.D. *Cryst Growth & Design* **2010**, *10*, 4728-4740.

(17) Groen H.; Mougin P.; Thomas A.; White G.; Wilkinson D.; Hammond R.B.; Lai X.; Roberts K.J. *Ind. Eng. Chem. Res.* **2003**, *42*, 4888-4898.

(18) Groen H.; Borissova A.; Roberts K. *J. Ind. Eng. Chem. Res.* **2003**, *42*, 198-206.

(19) Khan S.; Ma C.Y.; Mahmud T.; Penchev R.Y.; Roberts K.J.; Morris J.; Özkan L.; White G.; Grieve B.; Hall A.; Buser P.; Gibson N.; Keller P.; Shuttleworth P.; Price J.C. *Org. Proc. Res. & Dev.* **2011**, *15*, 540-555.

(20) Schlemmer, H. *Fresenius. Z. Anal. Chem.* **1987**, *329*, 435 -439.

(21) Thompson, D. R.; Kougoulosb, E.; Jonesb, A. G.; Wood-Kaczmara, M. W. *J. Cryst. Growth* **2005**, *276*, 230-236.

(22) Vernier Software & Technology, LLC.

(23) *CrysAlis CCD and CrysAlis RED. Oxford; Diffraction Ltd, Yarnton, England* **2009**.

(24) G.M. Sheldrick, *SHELXS97, Program for the Solution of Crystal Structures; University of Gottingen: Gottingen, Germany* **1997**.

(25) MacCalman M.L.; Roberts K.J.; Hendriksen B.A. J*. Cryst. Growth* **1993**, *128*, 1218-1224.

(26) Groen H.C.; Roberts K.J. *J. Phys. Chem. B* **2001**, *105*, 10723-10730.

(27) Borissova A.; Khan S.; Mahmud T.; Roberts K.J.; Andrews J.; Dallin P.; Chen Z.P.; Martin E.; Morris J. *Cryst. Growth Des.* **2009**, *9*, 692-706.

(28) van Gelder R.N.M.R.; Roberts K.J.; Chambers J.; Instone T.; *J. Cryst. Growth* **1996**, *166*, 189-194.

(29) Qu, H.; Louhi-Kultanen, M.; Kallasa J. *Int. J. Pharm.* **2006**, *321*, 101-107

List of symbols and abbreviations:

ATR-UVvis	Attenuated Total Reflection Ultraviolet/Visible Spectroscopy
Au(111)	Single crystal gold surface (111)
FBRM	Focus Beam Reflectance Measurement
MSZW	MetaStable Zone Width
PAT	Process Analytical Technology
XRD	X-Ray Diffraction

A	-	absorption
b	-	crystal growth factor
c	g/L	concentration
G	$\mu m\ s^{-1}$	growth rate
$\Delta_f H$	$Jmol^{-1}$	molar enthalpy of the fusion
$h\ k\ l$	-	Miller indexes
l	micro meters	chord length
k_G	-	growth rate coefficient
R	$JK^{-1}mol^{-1}$	gas constant
T	^oC	temperature
x	-	molar fraction of the solute in the solution
γ	g/L	mass concentration
σ	-	relative supersaturation